Acta Crystallographica Section F
Structural Biology and Crystallization Communications
ISSN 1744-3091

Structure of formaldehyde dehydrogenase from *Pseudomonas aeruginosa*: the binary complex with the cofactor NAD$^+$

Yuanping Liao,[a]‡ Shuai Chen,[a]‡ Dingli Wang,[a]‡ Wangluo Zhang,[a] Shuang Wang,[a] Jianfeng Ding,[a] Yingming Wang,[a] Lijun Cai,[a] Xiaoyuan Ran,[a] Xinquan Wang[b] and Huaxing Zhu[a]*

[a]R&D Department, Novoprotein Scientific Inc. (Shanghai), R202, Building 2, 720 Cailun Road, Shanghai 201203, People's Republic of China, and [b]Ministry of Education Key Laboratory of Protein Science, Center for Structural Biology, School of Life Sciences, Tsinghua University, Beijing 100084, People's Republic of China

‡ These authors contributed equally to this work.

Correspondence e-mail: zhuhuaxing@novoprotein.com.cn

Received 25 June 2013
Accepted 2 August 2013

PDB Reference: NAD$^+$-bound formaldehyde dehydrogenase, 4jlw

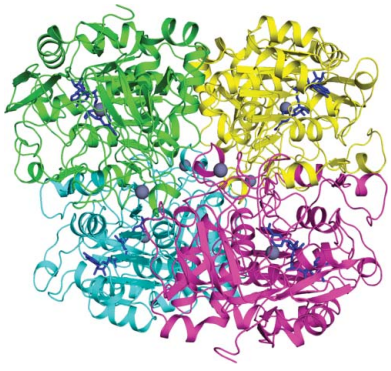

© 2013 International Union of Crystallography
All rights reserved

Formaldehyde dehydrogenase (FDH) is a member of the zinc-containing medium-chain alcohol dehydrogenase family which oxidizes toxic formaldehyde to formate using NAD$^+$ as an electron carrier. Three-dimensional structures have been reported for FDHs from several different species. Most FDHs are dependent on glutathione for catalysis, but the enzyme from *Pseudomonas putida* is an exception. In this structural communication, the recombinant production, crystallization and X-ray structure determination at 2.7 Å resolution of FDH from *P. aeruginosa* are described. Both the tetrameric assembly and the NAD$^+$-binding mode of *P. aeruginosa* FDH are similar to those of *P. putida* FDH, which is in good agreement with the high sequence identity (87.97%) between these two proteins. Preliminary enzymatic kinetics studies of *P. aeruginosa* FDH also revealed a conserved glutathione-independent 'ping-pong' mechanism of formaldehyde oxidization.

1. Introduction

Formaldehyde is a toxic compound and most organisms have developed oxidation systems to counteract it. An example is formaldehyde dehydrogenase (FDH), which catalyzes the oxidation of formaldehyde using NAD$^+$ as an electron acceptor and is found in both prokaryotes and eukaryotes (Uotila & Koivusalo, 1989). FDH belongs to the zinc-containing medium-chain alcohol dehydrogenase (ADH) family, which has long attracted interest in structural and functional studies (Persson *et al.*, 1991, 1994; Rossmann *et al.*, 1975).

Crystal structures of ADHs from a number of species have been reported, revealing the presence of either a dimer (Eklund *et al.*, 1981; Sanghani *et al.*, 2002) or a tetramer (Jenkins & Tanner, 2006; Cowan-Jacob *et al.*, 2003) as the active form, with each monomer (350–400 amino-acid residues) consisting of catalytic and coenzyme-binding domains together with two bound zinc ions. Functionally, most FDHs are known to be dependent on glutathione during catalysis of formaldehyde oxidation and the reaction product is actually *S*-formylglutathione rather than free formate (Rose & Racker, 1962; Johnson & Quayle, 1964; Strittmatter & Ball, 1955; Sanghani *et al.*, 2000). The FDH from *Pseudomonas putida* is the only member of the ADH family identified to date that can catalyze irreversible oxidation of formaldehyde without glutathione (Ando *et al.*, 1979; Ito *et al.*, 1994). In addition, the enzyme can catalyze aldehyde dismutation without releasing NAD(H) (Tanaka *et al.*, 2002). Its catalytic mechanism of aldehyde dismutation is distinct from most typical ADHs, which use NAD(H) as an exchangeable coenzyme. The crystal structure of this homotetrameric enzyme (Tanaka *et al.*, 2002) revealed a similar structural arrangement and similar binding modes of NAD$^+$ and zinc ions to these typical ADHs, except that *P. putida* FDH contains a number of different loop structures. In particular, a long insertion loop (residues 265–279) was found in the cofactor-binding domain and might contribute to the tight binding of the enzyme to NAD$^+$ during catalysis of aldehyde dismutation.

Here, we report the crystal structure of FDH from *P. aeruginosa* bound to the cofactor NAD$^+$ at 2.7 Å resolution. *P. aeruginosa* is a ubiquitous environmental Gram-negative bacterium and is a major pathogen that causes opportunistic human infections owing to its intrinsic resistance to antibiotics and disinfectants (Hardalo &

Edberg, 1997; Bodey *et al.*, 1983). The tetrameric form is observed in the crystal structure as well as in solution. Structural comparison with *P. putida* FDH indicated high similarity between these two enzymes. The enzymatic kinetics of *P. aeruginosa* FDH towards the substrate formaldehyde are also reported.

2. Experimental

2.1. Cloning, expression and purification

The FDH gene of *P. aeruginosa* (strain LESB58) was synthesized based on the protein sequence (residues 1–399; UniProt accession No. B7V5W2) and the DNA sequence was optimized to adapt codon usage to the expression host using *JCat* (Grote *et al.*, 2005). An N-terminal His tag (MNHKVHHHHHH) was also introduced into the protein. The synthesized DNA was inserted between the *Nde*I and *Hin*dIII sites of the pCold II vector (Takara) and the resulting plasmid was transformed into *Escherichia coli* BL21(DE3)/pG-TF2 cells (Novoprotein), which contain a coexpression system for the chaperones GroEL, GroES and Tig. Cultures were grown in LB medium containing ampicillin (100 µg ml^{-1}) and chloramphenicol (34 µg ml^{-1}) at 310 K to an OD_{600} of 0.5–0.6; 10 ng ml^{-1} tetracycline was then introduced to produce the chaperones for 30 min. The His-tagged FDH protein was then produced at 289 K for 12 h after adding 0.2 m*M* IPTG to the culture.

Freeze–thawed cell pellets were resuspended in lysis buffer (20 m*M* Tris–HCl pH 8.0, 250 m*M* NaCl, 20 m*M* imidazole) and disrupted by sonication on ice. The crude lysate was centrifuged at 12 000*g* for 30 min and the supernatant was filtered through a 0.45 µm filter and loaded onto a pre-equilibrated 5 ml Ni–NTA column (GE Healthcare). The column was washed with 20 column volumes of lysis buffer and eluted with an imidazole gradient (50–250 m*M*). The eluted samples were then dialyzed against buffer *A* (20 m*M* Tris–HCl pH 8.0, 1 m*M* DTT) and further loaded onto a 10 ml Mono Q FF column (GE Healthcare) pre-equilibrated with buffer *A*. The column was washed with buffer *A* and was then eluted with a NaCl gradient (0.05–1.0 *M*) in buffer *A*. Peak fractions containing FDH were pooled and concentrated to 20 mg ml^{-1}. Finally, the purified and concentrated FDH was dialyzed against 10 m*M* Tris–HCl pH 8.0, 1 m*M* DTT, which was used as crystallization buffer, and stored at 253 K.

The multimeric state of *P. aeruginosa* FDH was analyzed by size-exclusion chromatography (SEC) on a HiLoad 26/60 Superdex 200 column (GE Healthcare). Protein samples at a concentration of 2 mg ml^{-1} were loaded onto the column and were eluted with buffer *A* (20 m*M* Tris–HCl pH 8.0, 1 m*M* DTT), with detection of the absorbance at 280 nm.

2.2. Enzymatic activity assay

As described by the equation

$$\text{formaldehyde} + \text{NAD}^+ + \text{H}_2\text{O} \xrightarrow{\text{FDH}} \text{formate} + \text{NADH} + \text{H}^+,$$

the enzymatic activity of the FDH was assayed by measuring the formation of NADH in terms of the increase in absorbance at 340 nm (Ando *et al.*, 1979). A 0.1 ml aliquot of the enzyme (20 µg ml^{-1}) was incubated with 1 ml formaldehyde at various concentrations and NAD^+ (20–500 µ*M*) in 50 m*M* potassium phosphate buffer pH 7.5 at 298 K in a quartz cuvette with 1 cm path length. The change in absorbance at 340 nm was monitored against a blank test at 2 min intervals using a UV-7504 spectrophotometer (Shanghai Xinmao Instrument Co. Ltd). The formation of NADH as a function of time was expressed as $\Delta E_{340\,\text{nm}}$ min^{-1}. The initial reaction velocity (v_0) was determined from the linear part of the curve and was averaged over three independent assays. The Michaelis constants (K_m) of the enzyme for formaldehyde and NAD^+ were calculated from a Lineweaver–Burk plot based on a bi-substrate kinetics model.

Table 1
Data-collection and refinement statistics for FDH–NAD^+.

Values in parentheses are for the highest resolution shell.

Data-collection statistics	
Wavelength (Å)	0.9791
Resolution (Å)	50.00–2.70 (2.80–2.70)
Space group	$P2_1$
Molecules per asymmetric unit	4
Unit-cell parameters (Å, °)	a = 89.23, b = 98.31, c = 99.62, $\alpha = \gamma$ = 90.00, β = 91.29
No. of observed reflections	168470
No. of unique reflections	47323 (4719)
Data multiplicity	3.6 (3.6)
Completeness (%)	99.8 (99.9)
Mean $I/\sigma(I)$	6.43 (2.91)
R_{merge}† (%)	20.3 (63.4)
Refinement statistics	
Resolution (Å)	30.00–2.70 (2.77–2.70)
No. of reflections/No. in test set	44912/2394
Completeness (%)	99.30 (92.98)
$R_{\text{work}}/R_{\text{free}}$‡ (%)	21.18/25.94
No. of atoms	
Protein	11704
Ligand/ion	214
Water	454
Modelled residues§	
Chains *A*–*D*	3–397
Overall *B* factor (Å^2)	
Protein	27.05
Ligand/ion	35.13
Water	26.13
R.m.s.d., bond lengths¶ (Å)	0.012
R.m.s.d., bond angles¶ (°)	1.641
Ramachandran plot, residues in†† (%)	
Favoured region	97.1
Allowed region	2.9
Outlier region	0

† $R_{\text{merge}} = \sum_{hkl}\sum_i |I_i(hkl) - \langle I(hkl)\rangle| / \sum_{hkl}\sum_i I_i(hkl)$, where $I_i(hkl)$ and $\langle I(hkl)\rangle$ are the ith and the mean measurement of the intensity of the unique reflection hkl, respectively. ‡ $R_{\text{work}} = \sum_{hkl} ||F_{\text{obs}}| - |F_{\text{calc}}|| / \sum_{hkl} |F_{\text{obs}}|$, where F_{obs} and F_{calc} are the observed and calculated structure-factor amplitudes for reflection hkl and the summation is over 95% of the reflections in the specified resolution range. The remaining 5% of the reflections were randomly selected before structure refinement and were not included in the structure refinement. R_{free} was calculated over these reflections using the same equation as for R_{work}. § The N-terminal His tag and residues 1–2 and 398–399 of FDH were omitted from the final model owing to poorly resolved electron density. ¶ Root-mean-square deviations from the parameter set for ideal stereochemistry. †† As defined by *MolProbity*.

2.3. Crystallization

To generate the FDH–NAD^+ complex, the concentrated FDH was incubated with a solution of NAD^+ (dissolved in 10 m*M* Tris–HCl pH 8.0, 1 m*M* DTT) at 277 K for 2 h. The protein–NAD^+ solution consisting of 15 mg ml^{-1} FDH and 4 mg ml^{-1} NAD^+ in 10 m*M* Tris–HCl pH 8.0, 1 m*M* DTT was then used for crystallization trials. All crystallization screenings were performed at 291 K using the sitting-drop vapour-diffusion method and each drop (1 µl) was prepared by mixing equal volumes of protein–NAD^+ solution and reservoir solution. Initial hits were obtained using commercially available crystallization screening kits (Hampton Research Crystal Screen and Crystal Screen 2). Subsequent optimization was performed by setting up 2 µl drops consisting of 1 µl protein–NAD^+ solution and 1 µl reservoir solution, and crystals of the FDH–NAD^+ complex grew in 0.1 *M* bis-tris pH 5.5–6.5, 1.5–2.5 *M* ammonium sulfate at 291 K. Optimum plate-shaped crystals (100 × 50 × 20 µm) were obtained from 0.1 *M* bis-tris pH 5.5, 1.8 *M* ammonium sulfate after several rounds of streak-seeding using a cat whisker.

2.4. Data collection and processing

The crystals were cryoprotected in 0.1 *M* bis-tris pH 5.5, 2.0 *M* ammonium sulfate with 20%(*v*/*v*) glycerol and were harvested into nylon loops prior to flash-cooling in liquid nitrogen. Diffraction data were collected at 100 K with an ADSC Q315 CCD detector using synchrotron radiation (λ = 0.9791 Å) on beamline BL17U at the Shanghai Synchrotron Radiation Facility (SSRF; Shanghai, People's Republic of China). The crystal diffracted to 2.7 Å resolution and all data processing was performed with *HKL*-2000 (Otwinowski & Minor, 1997).

2.5. Structure solution and refinement

The structure of *P. putida* FDH (PDB entry 1kol, chain *A*; Tanaka *et al.*, 2002) was selected as the search model for molecular replacement. The bound NAD^+ and all solvent molecules were removed from the model and molecular replacement was carried out with *Phaser* (McCoy *et al.*, 2007). Model refinement was performed with *REFMAC*5 (Murshudov *et al.*, 2011) followed by employing *Coot* (Emsley & Cowtan, 2004) for iterative cycles of rebuilding based on σ_A-weighted $2F_o - F_c$ and $F_o - F_c$ maps. Noncrystallographic symmetry (NCS) restraints were applied to chains *A* and *D* and to chains *B* and *C* in the early stages of refinement. Solvent molecules were identified based on the $F_o - F_c$ difference map. The final steps of refinement also incorporated TLS restraints (Painter & Merritt, 2006); a total of 19 TLS groups were selected, which were automatically determined by *PHENIX* (Adams *et al.*, 2010). The stereochemical quality of the refined structure was validated using *MolProbity* (Chen *et al.*, 2010). Data-collection and refinement statistics are presented in Table 1. The interfaces of the FDH tetramer were analyzed using *PDBePISA* (http://www.ebi.ac.uk/msd-srv/prot_int/pistart.html; Krissinel & Henrick, 2007). Global alignment of the FDH structures was performed using *PyMOL* (super_align; Schrödinger) and all structural model figures were also created with *PyMOL*. Structure factors and coordinates have been deposited in the Protein Data Bank (http://www.rcsb.org/pdb) under accession code 4jlw.

3. Results and discussion

3.1. Crystallization, data collection and structure determination

Crystals of FDH from *P. aeruginosa* bound to the cofactor NAD^+ were obtained by the sitting-drop vapour-diffusion method. The crystals belonged to the monoclinic space group $P2_1$, with unit-cell parameters a = 89.23, b = 98.31, c = 99.62 Å, β = 91.29°. A total of four molecules were observed per asymmetric unit, giving a V_M value of 2.62 $Å^3$ Da^{-1} and a solvent content of 52% (Matthews, 1968). The structure was solved by molecular replacement using the *P. putida* FDH structure as a search model. Iterative refinement and manual building of the model resulted in a final R_{work} of 21.18% and an R_{free} of 25.94%. Electron density corresponding to residues 3–397, one NAD^+ molecule and two zinc ions was well defined for each of the four crystallographically independent protein subunits. In addition, a total of 454 water molecules and six sulfate ions were included per asymmetric unit. A Ramachandran plot of the final model indicated that 97.1% of the residues were in mostly favoured regions and 2.9% were in additionally allowed regions.

3.2. The overall structure of *P. aeruginosa* FDH

As depicted in Fig. 1(*a*), the final model of *P. aeruginosa* FDH consists of four protein subunits forming a homotetramer with a total buried surface area of ~12 920 $Å^2$. The tetramer could be considered as a dimer of dimers formed by subunits *A* (green) and *B* (cyan) and by subunits *C* (magenta) and *D* (yellow). Analogous dimeric interactions have been reported in the structures of mammalian ADHs (Eklund *et al.*, 1981; Sanghani *et al.*, 2002). The interface of the *A*–*B* (or *C*–*D*) dimer is mainly composed of a six-stranded parallel β-sheet from each subunit and has a total buried surface area of ~3300 $Å^2$. In forming the tetramer, the *A*–*B* dimer contacts the *C*–*D* dimer by two types of subunit–subunit interfaces. One interface is between subunit *A* (green) and subunit *C* (magenta), with a total buried surface area of ~1600 $Å^2$. The other interface is formed by subunit *A* (green) and

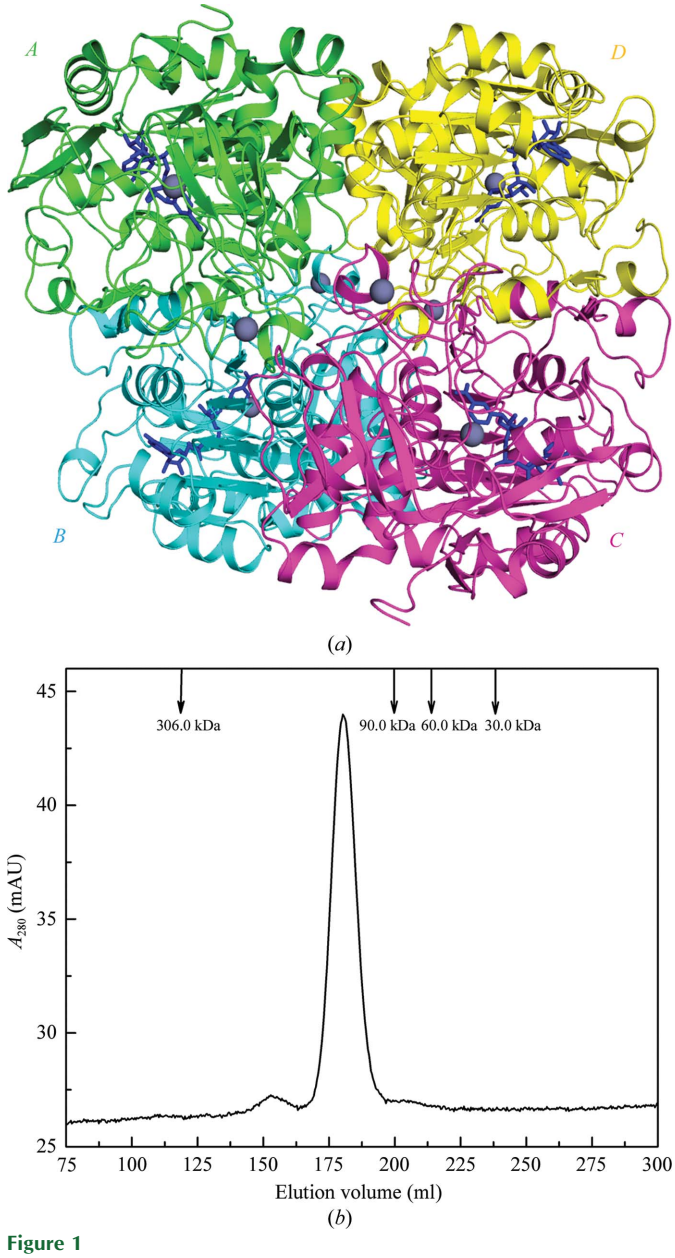

Figure 1
Tetrameric NAD^+-bound formaldehyde dehydrogenase (FDH) from *P. aeruginosa*. (*a*) The overall structure of the FDH tetramer. Four subunits (*A*–*D*) are shown in ribbon mode in different colours. The zinc ions are depicted as grey spheres and the bound NAD^+ ions are shown as blue sticks for each of the four subunits. (*b*) SEC analysis of the FDH at a concentration of 2 mg ml^{-1}. The protein sample was loaded onto a HiLoad 26/60 Superdex 200 column and was eluted at a flow rate of 3 ml min^{-1} with detection of the absorbance at 280 nm. The elution profiles of four molecular-mass protein standards are also shown as labelled arrows.

subunit *D* (yellow) and possesses a total buried surface area of ~1500 Å^2 (Fig. 1*a*). The tetrameric assembly observed here also appears in the structure of *P. putida* FDH through the [210] crystallographic symmetry operation (Tanaka *et al.*, 2002). In order to determine whether the tetramer corresponds to a natural state in solution, SEC analysis was performed (Fig. 1*b*). The protein eluted as a single peak with a retention volume of 180.3 ml, corresponding to an estimated molecular mass of ~150 kDa. This further implies that

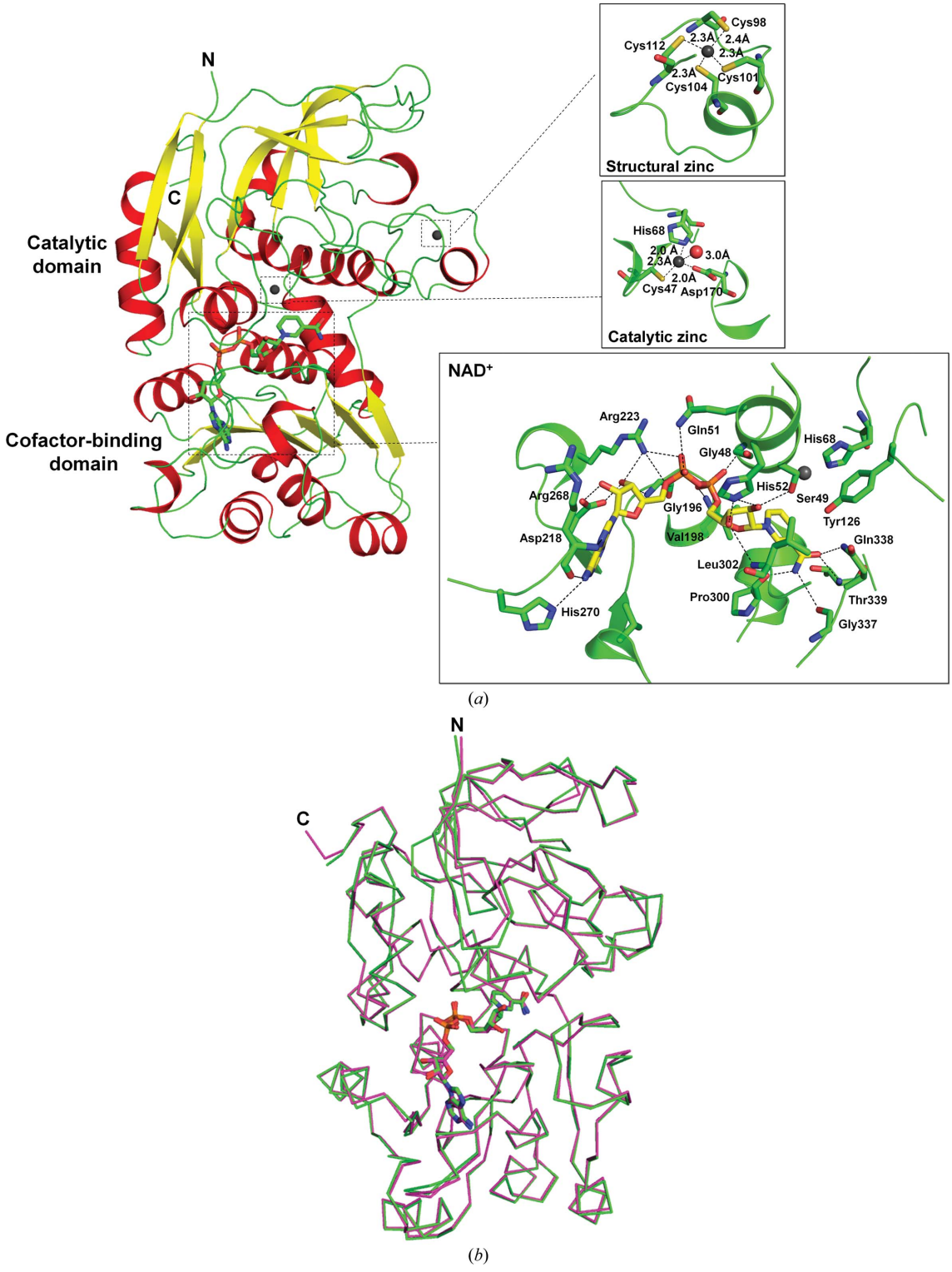

Figure 2
The structure of the *P. aeruginosa* FDH subunit. (*a*) Ribbon drawing of FDH subunit *A*. The N- and C-termini are labelled by the letters N and C, respectively. α-Helices are coloured red, β-strands yellow and loops green. The NAD$^+$ and zinc ions are highlighted as sticks and spheres, respectively. The insets show the binding modes of two zinc ions (grey spheres) and the cofactor NAD$^+$ (sticks) to the FDH subunit. Hydrogen bonds are indicated by dotted lines. The residues of FDH involved in binding are shown as sticks and the residue numbers are indicated. (*b*) Superimposition of FDH subunit *A* (green) with a subunit of *P. putida* FDH (magenta). Proteins are indicated by C$^\alpha$ traces with N- and C-termini marked and the bound NAD$^+$ ions are shown in stick representation.

the enzyme exists in a tetrameric form since the theoretical molecular mass of monomeric *P. aeruginosa* FDH is 43.4 kDa.

Similar to other ADHs, each subunit of *P. aeruginosa* FDH is composed of two domains separated by a cleft containing a deep pocket (Fig. 2*a*). Both the N-terminus (residues 1–2) and C-terminus (residues 398–399) of the FDH subunit along with its N-terminal His tag (MNHKVHHHHHH) are not visible in the electron density and were not included in the final model. One of the domains (residues 3–170 and 339–397) is responsible for the binding and catalysis of formaldehyde and is named the catalytic domain; the other domain (residues 171–338) that provides the structural moiety necessary for NAD^+ binding is designated the cofactor-binding domain. The catalytic domain mainly consists of eight β-strands and seven α-helices, and all of the α-helices are aligned on the surface of the domain to surround the β-structural core. For the cofactor-binding domain, the overall arrangement of its secondary structures is a six-stranded parallel β-sheet sandwiched by three α-helices on either side, which comprises a characteristic 'Rossmann fold' (Rossmann *et al.*, 1974). The cofactor NAD^+ is bound to the central region of the carboxyl end of the parallel β-sheet. A structural comparison of the FDH subunit (chain *A*) with the structure of *P. putida* FDH (PDB entry 1kol, chain *A*) yielded a root-mean-square (r.m.s.) distance of 0.23 Å for all 395 equivalent C^α atoms (Fig. 2*b*), indicating high structural similarity between these two FDHs from different *Pseudomonas* bacterial strains.

3.3. Zinc- and NAD^+-binding sites

In the current FDH structure, two firmly bound zinc ions were observed per subunit (Fig. 2*a*, inset). One zinc ion, the so-called structural zinc, is coordinated to the S atoms of Cys98, Cys101, Cys104 and Cys112 from the catalytic domain. Its tetrahedral coordination geometry is well ordered owing to similar zinc–ligand distances among the four Cys ligands (~2.3 Å). The other zinc ion, called the catalytic zinc, is located at the bottom of the cleft between the two domains of the FDH subunit and has a tetrahedral coordination environment with Cys47, His68 and Asp170 as the three protein ligands together with a water molecule. Compared with the structural zinc, the tetrahedral geometry of the catalytic zinc is more distorted, which might be caused by unequal zinc–ligand distances among the different ligand elements (sulfur, nitrogen and oxygen).

In addition to the two zinc ions, the overall conformation of the cofactor NAD^+ and its binding mode to the FDH subunit in the present structure are also similar to those observed for *P. putida* FDH (Fig. 2*b*). The bound NAD^+ adopts an *anti* conformation, with the nicotinamide and adenine rings orientated roughly perpendicular to the planes of their respective ribose rings (Fig. 2*a*, inset). The nicotinamide nucleoside moiety of the NAD^+ interacts with the FDH through eight hydrogen bonds. Four hydrogen bonds are formed from the carboxamide group of the nicotinamide ring to the protein main chain (NAD^+ N7N···Pro300 O, NAD^+ N7N···Gly337 O and NAD^+ O7N···Thr339 N) and side chain (NAD^+ O7N···Gln338 NE2). The other four were observed between the hydroxyl groups of the ribose ring and the protein: NAD^+ O2D···Ser49 OG, NAD^+ O2D···His52 NE2, NAD^+ O3D···His52 NE2 and NAD^+ O3D···Leu302 N. In addition, the pyrophosphate moiety of the NAD^+ is hydrogen-bonded to the FDH between the O atoms of the nicotinamide or adenine phosphate groups and several protein residues, *e.g.* NAD^+ O1N···Gly48 N, NAD^+ O2N···Val198 N, NAD^+ O1A···Arg223 NH1, NAD^+ O2A···Gln51 NE2 and NAD^+ O5B···Arg223 NH1. Meanwhile, the adenine ribose moiety of the NAD^+ also forms extensive interactions with the FDH subunit. In detail, the 2′- and 3′-hydroxyl groups of the ribose ring are recognized by the side chain of Asp218 to form a bifurcated hydrogen bond (NAD^+ O2B···Asp218 OD1 and NAD^+ O3B···Asp218 OD2). Two other hydrogen bonds are observed between the ribose ring and residues Gly196 and Arg223 (NAD^+ O3B···Gly196 N and NAD^+ O3B···Arg223 NH1). Furthermore, the adenine ring is accommodated in a network of hydrogen bonds which is constituted by the N atoms of the adenine ring and the main chain of Arg268 (NAD^+ N6A···Arg268 O and NAD^+ N7A···Arg268 N), as well as the amino group of the adenine ring and the side chain of His270 (NAD^+ N6A···His270 NE2).

3.4. The enzymatic kinetics of *P. aeruginosa* FDH

As mentioned above, *P. putida* FDH is the only identified ADH that is independent of glutathione for catalysis (Ando *et al.*, 1979). Considering the similarity of our structure to that of *P. putida* FDH, the enzymatic activity of *P. aeruginosa* FDH towards the substrate formaldehyde was therefore measured. Firstly, the enzyme required only NAD^+ as an electron carrier and addition of glutathione had no effect on the reaction rate (data not shown), indicating glutathione-independent catalysis. The reactions were then kinetically assayed and the results are shown in Fig. 3. Initial double-reciprocal plots of the reaction velocity *versus* formaldehyde produced nearly parallel lines for various concentrations of NAD^+, implying that the reaction proceeds by a 'ping-pong' mechanism as designated by the Michaelis–Menten model of bi-substrate enzymatic kinetics (Cleland, 1967). The K_m values for formaldehyde and NAD^+ are 15.3 and 55.0 μM, respectively, which were calculated from the initial plots together with a secondary plot of the intercepts of the parallel lines against the reciprocal of the concentration of NAD^+. These results are also comparable with the published data for *P. putida* FDH (Ando *et al.*, 1979).

In summary, in this communication we have presented the binary-complex structure of *P. aeruginosa* FDH bound to the cofactor NAD^+

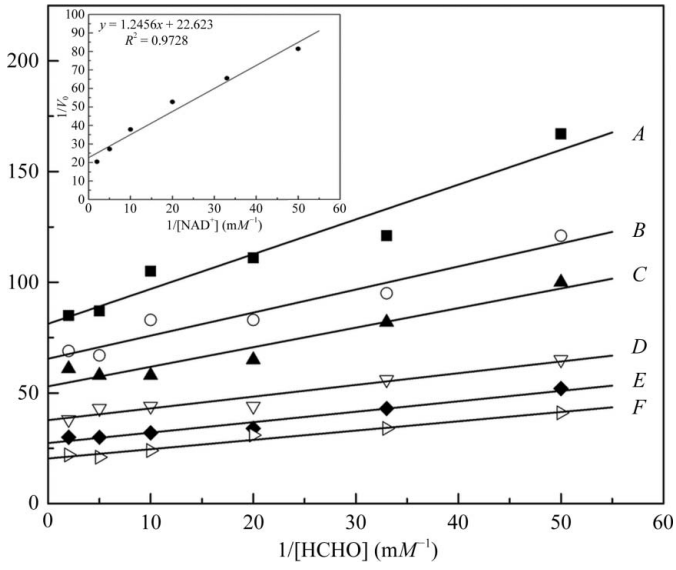

Figure 3
Enzymatic activity of *P. aeruginosa* FDH towards the substrate formaldehyde. Double-reciprocal plots of the reaction catalyzed by FDH as a function of the concentration of formaldehyde are shown. The enzyme was incubated with various concentrations of formaldehyde (20–500 μM) and the change in absorbance at 340 nm was monitored. The reaction velocity was expressed as $\Delta E_{340\ nm}$ min^{-1}. The concentrations of NAD^+ were *A*, 20 μM; *B*, 30 μM; *C*, 50 μM; *D*, 100 μM; *E*, 200 μM; *F*, 500 μM. The inset shows a secondary plot of the intercepts of the parallel lines *versus* the reciprocal of the concentration of NAD^+.

as well as the preliminary characterization of its enzymatic kinetics. Consistent with the published results for the homologous structure of *P. putida* FDH, the enzyme shows well conserved structural and catalytic features. It will be of interest to determine the structure of a ternary complex of the enzyme with NAD^+ and formaldehyde in the future, which could further elucidate the detailed mechanism of glutathione-independent catalysis.

We are grateful to Li Wang and members of our company for critically reading the manuscript.

References

Adams, P. D. *et al.* (2010). *Acta Cryst.* D**66**, 213–221.
Ando, M., Yoshimoto, T., Ogushi, S., Rikitake, K., Shibata, S. & Tsuru, D. (1979). *J. Biochem.* **85**, 1165–1172.
Bodey, G. P., Bolivar, R., Fainstein, V. & Jadeja, L. (1983). *Rev. Infect. Dis.* **5**, 279–313.
Chen, V. B., Arendall, W. B., Headd, J. J., Keedy, D. A., Immormino, R. M., Kapral, G. J., Murray, L. W., Richardson, J. S. & Richardson, D. C. (2010). *Acta Cryst.* D**66**, 12–21.
Cleland, W. W. (1967). *Annu. Rev. Biochem.* **36**, 77–112.
Cowan-Jacob, S. W., Kaufmann, M., Anselmo, A. N., Stark, W. & Grütter, M. G. (2003). *Acta Cryst.* D**59**, 2218–2227.
Eklund, H., Samama, J.-P., Wallén, L., Brändén, C. I., Åkeson, Å. & Jones, T. A. (1981). *J. Mol. Biol.* **146**, 561–587.
Emsley, P. & Cowtan, K. (2004). *Acta Cryst.* D**60**, 2126–2132.
Grote, A., Hiller, K., Scheer, M., Münch, R., Nörtemann, B., Hempel, D. C. & Jahn, D. (2005). *Nucleic Acids Res.* **33**, W526–W531.
Hardalo, C. & Edberg, S. C. (1997). *Crit. Rev. Microbiol.* **23**, 47–75.
Ito, K., Takahashi, M., Yoshimoto, T. & Tsuru, D. (1994). *J. Bacteriol.* **176**, 2483–2491.
Jenkins, J. L. & Tanner, J. J. (2006). *Acta Cryst.* D**62**, 290–301.
Johnson, P. A. & Quayle, J. R. (1964). *Biochem. J.* **93**, 281–290.
Krissinel, E. & Henrick, K. (2007). *J. Mol. Biol.* **372**, 774–797.
Matthews, B. W. (1968). *J. Mol. Biol.* **33**, 491–497.
McCoy, A. J., Grosse-Kunstleve, R. W., Adams, P. D., Winn, M. D., Storoni, L. C. & Read, R. J. (2007). *J. Appl. Cryst.* **40**, 658–674.
Murshudov, G. N., Skubák, P., Lebedev, A. A., Pannu, N. S., Steiner, R. A., Nicholls, R. A., Winn, M. D., Long, F. & Vagin, A. A. (2011). *Acta Cryst.* D**67**, 355–367.
Otwinowski, Z. & Minor, W. (1997). *Methods Enzymol.* **276**, 307–326.
Painter, J. & Merritt, E. A. (2006). *Acta Cryst.* D**62**, 439–450.
Persson, B., Krook, M. & Jörnvall, H. (1991). *Eur. J. Biochem.* **200**, 537–543.
Persson, B., Zigler, J. S. & Jörnvall, H. (1994). *Eur. J. Biochem.* **226**, 15–22.
Rose, Z. B. & Racker, E. (1962). *J. Biol. Chem.* **237**, 3279–3281.
Rossmann, M. G., Lijas, A., Brändén, C.-I. & Banaszak, L. J. (1975). *The Enzymes*, 3rd ed., edited by P. D. Boyer, Vol. XI, pp. 61–102. New York: Academic Press.
Rossmann, M. G., Moras, D. & Olsen, K. W. (1974). *Nature (London)*, **250**, 194–199.
Sanghani, P. C., Robinson, H., Bosron, W. F. & Hurley, T. D. (2002). *Biochemistry*, **41**, 10778–10786.
Sanghani, P. C., Stone, C. L., Ray, B. D., Pindel, E. V., Hurley, T. D. & Bosron, W. F. (2000). *Biochemistry*, **39**, 10720–10729.
Strittmatter, P. & Ball, E. G. (1955). *J. Biol. Chem.* **213**, 445–461.
Tanaka, N., Kusakabe, Y., Ito, K., Yoshimoto, T. & Nakamura, K. T. (2002). *J. Mol. Biol.* **324**, 519–533.
Uotila, L. & Koivusalo, M. (1989). In *Glutathione: Chemical, Biochemical, and Medical Aspects*, Part A, edited by D. Dolphin, R. Poulson & O. Avramovic. New York: Wiley.